Journal of Alloys and Compounds 678 (2016) 325–328

Contents lists available at ScienceDirect

Journal of Alloys and Compounds

journal homepage: http://www.elsevier.com/locate/jalcom

Origin of the strain glass transition in $Ti_{50}(Ni_{50-x}\ D_x)$ alloys

Xu Wang [a], Jia-Xiang Shang [a, *], Fu-He Wang [b], Yue Chen [c, **]

[a] School of Materials Science and Engineering, Beihang University, Beijing, 100191, China
[b] Department of Physics, Capital Normal University, Beijing, 100048, China
[c] Department of Mechanical Engineering, The University of Hong Kong, Pokfulam Road, Hong Kong SAR, China

ARTICLE INFO

Article history:
Received 30 November 2015
Received in revised form
23 March 2016
Accepted 30 March 2016
Available online 1 April 2016

Keywords:
First-principles calculation
Structural phase transition
Ti–Ni-based alloys
Strain glass transition

ABSTRACT

Direct evidence was recently discovered for the unique strain glass (STG) transition, which breaks the local symmetries (PRL 112, 025701 (2014)). To understand the origin of the STG transition, the effects of doping point defects on $Ti_{50}(Ni_{50-x}\ D_x)$ are investigated using first-principle calculations. The experimental observation that STG only exists in a limited range of chemical composition x is successfully rationalized. The mechanisms that correspond to the division of a system into domains with distinctly different compositions are found to be directly related to a dip in the defect formation energy.

Strain glass (STG) is a novel glassy state which was discovered in Ni-rich $Ti_{50-x}\ Ni_{50+x}$ ferroelastic alloys [1]. When the doping concentration x is higher than the critical level x_c, instead of transforming to a long-range ordered martensitic phase, the system freezes into a configuration of uncorrelated nano-clusters of martensitic phase distributed randomly in the austenitic B2 matrix, which is the so called STG [2–7]. Surprisingly, this non-martensitic strain glass can also exhibit the shape memory effect (SME) and the superelastic effect (SE) based on the stress-induced strain glass to martensitic phase transition [8,9], which may significantly enhance the regime of SME and SE. The STG results from a nanoscale displacive transition that breaks the local symmetries but maintains the average crystal structures, and this kind of transitions have been investigated based on simulations and theoretical modelings [10,11]. A direct observation of the STG and its freezing process at the atomic scale in $Ti_{50}(Pd_{41}\ Cr_9)$ were realized recently using the high resolution transmission electron microscopy (HREM) [12]. Based on the HREM observations, a new model for the STG was proposed; it was believed that the STG can be divided into two domains, which include the distorted B2 phase with high doping concentrations and the frozen martensitic nanoclusters with low doping concentrations.

The direct observation of STG is a significant advancement in the related research fields, however, the fundamental understanding of the STG transitions is lagging behind. The existence of STG has been mainly attributed to the local strain induced by doping point defects [13], however, there are many dopants which create local strains but do not induce STG, such as Pd [14,15], Pt [16] and Cu [17,18]. Zhou et al. [19] have also pointed out similar issues in the study of $Ti_{50}\ Ni_{50-x}\ D_x$, where D = Cr, Co or Mn. It is thus of great significance to have a better understanding of the STG transition in order to extend the scopes of application for related alloys. To clarify the different STG transition behaviors of the $Ti_{50}\ Ni_{50-x}\ D_x$ systems with different dopants, the transformation temperatures (T_M) are summarized as functions of doping concentrations in Fig. 1.

The doping effects are shown for some of the typical elements, which are usually considered to improve the properties of the Ti–Ni alloys. Pt and Pd are responsible for increasing the transformation temperature T_M of the Ti–Ni alloys [14–16], while Cu is mainly for the improvement of the mechanical properties, although it also slightly increases the T_M [17,18]. For this group of dopants, STG transitions do not exist in the $Ti_{50}\ Ni_{50-x}\ D_x$ alloys; a high doping concentration will change the phase transitions from B2→B19′ to B2→B19. On the other hand, significantly different behaviors of Cr, Mn, Fe and Co are observed in the $Ti_{50}\ Ni_{50-x}\ D_x$ alloys; the transformation temperature T_M decreases with increasing doping concentrations. At high concentrations of Cr, Mn, Fe or Co, the normal martensitic phase transition (MPT) is replaced

* Corresponding author.
** Corresponding author.
E-mail addresses: shangjx@buaa.edu.cn (J.-X. Shang), yuechen@hku.hk (Y. Chen).

http://dx.doi.org/10.1016/j.jallcom.2016.03.298
0925-8388/

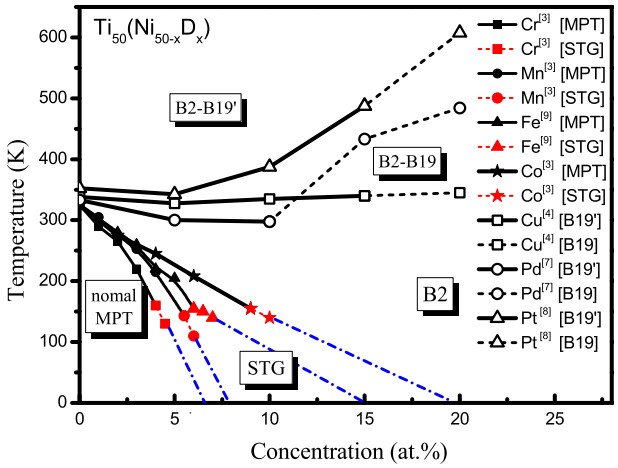

Fig. 1. The experimental transformation temperatures of $Ti_{50}(Ni_{50-x}D_x)$ as a function of the doping concentration *x*. The blue lines represent the extrapolations of the experimental data. (For interpretation of the references to color in this figure legend, the reader is referred to the web version of this article.)

by the STG transition [19–21]. To better understand the origins of these different behaviors, we have performed detailed investigations from first-principles calculations.

In this letter, we have chosen the $Ti_{50}(Ni_{50-x}D_x)$ alloys as our model systems; typical doping point defects that can (D = Cr, Mn, Fe, and Co) or cannot (D = Cu and Pd) induce the STG transition are investigated. The phase stability and transition behaviors of these alloys are studied based on density functional theory (DFT). According to the experimental results, we have focused on the B19′ and R structures for the martensitic phase of the alloys doped with Cr, Mn, Fe, or Co [19–21]. On the other hand, the B19′ and B19 structures are studied for the alloys doped with Cu or Pd [14,15,17,18]. A $2 \times 2 \times 3$ supercell of the B19′ and B19 structures, and a $1 \times 1 \times 2$ supercell of the R structure are constructed to study the transition behaviors as a function of doping concentration; doping point defects are distributed uniformly in the systems.

All calculations were performed with a projector-augmented wave (PAW) [22] approach as implemented in the Vienna *ab initio* simulation package (VASP) [23,24]. The cutoff energy of the plane wave is 500 eV. The generalized gradient approximation (GGA) by Perdew, Burke and Ernzerhof (PBE) [25] is used for the exchange-correlation potentials. The integration in the Brillouin zone is performed on a grid of $(5 \times 5 \times 5)$ Monkhorst-Pack k-points [26] for the $2 \times 2 \times 3$ supercell of the B19′ and B19 structures; a $(5 \times 5 \times 3)$ k-point mesh is applied for the $1 \times 1 \times 2$ supercell of the R structure.

The transformation behaviors as a function of the doping concentration can be described by the energy differences between the martensitic (the B19′, B19 or R structure) and the austenitic phases (the B2 structure): $\Delta E = E_M - E_A$. The martensitic transformation temperature (T_M) is closely related to the value of ΔE, as have been shown by Chen et al. [27]; it is found that T_M usually increases with decreasing ΔE. We have calculated the ΔE of the $Ti_{50}(Ni_{50-x}D_x)$ systems, with D = Cr, Mn, Fe, Co, Cu and Pd; the results are shown as a function of doping concentration in Fig. 2.

A similar transition behavior of the $Ti_{50}(Ni_{50-x}D_x)$ alloys with D = Cr, Mn, Fe and Co can be seen from Fig. 2(a–d). For increasing doping concentration *x*, $\Delta E_{B19'/R}$ increases monotonically, indicating a decrease in the MPT temperature T_M. At low doping concentrations, B19′ is the most stable martensitic phase, and the alloys may undergo a two-stage transition of B2→R→B19′, as $\Delta E_{B19'} < \Delta E_R < 0$. Although both of $\Delta E_{B19'}$ and ΔE_R increase with *x*, the different slopes

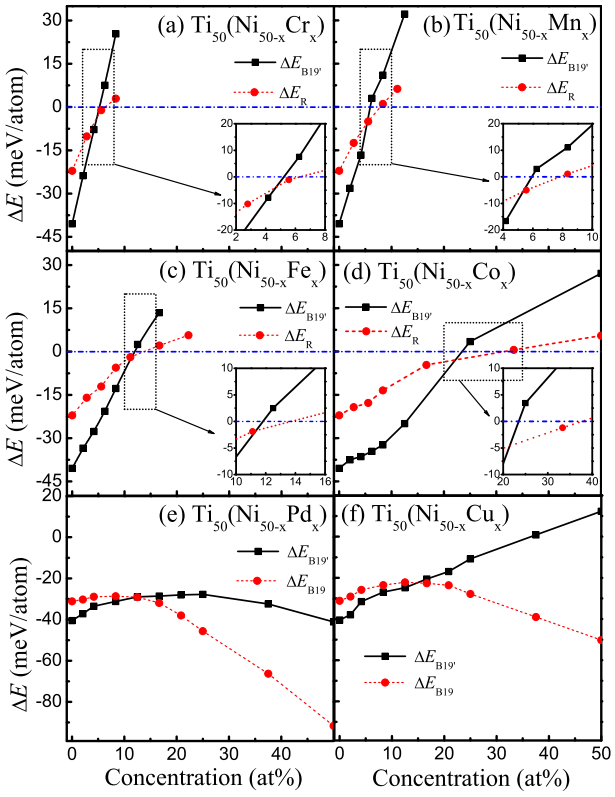

Fig. 2. The energy differences between the austenite and the martensite (ΔE) as a function of the doping concentration in $Ti_{50}(Ni_{50-x}D_x)$.

eventually make ΔE_R lower than $\Delta E_{B19'}$, as shown in the insets of Fig. 2(a–d); this also indicates that the R phase becomes the most stable martensitic phase and the MPT becomes B2→R. Consistent behaviors in the MPT have also been observed in experiments [19–21]. With *x* further increasing, both of $\Delta E_{B19'}$ and ΔE_R become positive; therefore, the B2 phase becomes the most stable structure, and MPT is completely suppressed. According to the experimental results [19–21], the STG transition takes place when the MPT is suppressed. Thus, in our calculations, the complete suppression of the MPT may indicate the existence of STG states in these alloys.

On the other hand, completely different behaviors of the $Ti_{50}(Ni_{50-x}D_x)$ alloys with D = Pd or Cu are identified through the computations of ΔE, as shown in Fig. 2(e) and (f). At low doping concentrations, $\Delta E_{B19'} < \Delta E_{B19} < 0$ and $\Delta E_{B19'}$ increases slightly with increasing *x*, suggesting a MPT of B2→(B19→) B19′ and the T_M decreases slightly with increasing *x*. At high doping concentrations, ΔE_{B19} decreases significantly and becomes lower than $\Delta E_{B19'}$; in other words, B19 becomes the most stable martensitic phase at high doping concentrations. The MPT thus becomes B2→B19, and the corresponding T_M increases significantly. These calculations are also in agreement with experimental results [14,15,17,18], as summarized in Fig. 1. In the mean time, it is worth noting that the STG state cannot be observed at any doping concentrations of Pd and Cu, instead, the long-range ordered martensitic B19′ and B19 phases emerge at low temperature. Therefore, by comparing our calculations with experiments, we find that only the doping point defects that completely suppress MPT can induce the STG transition.

The electronic origins of the suppression effects of Cr, Mn, Fe and Co on the MPT are investigated; the partial density of states (PDOS) of the austenitic phase with a doping concentration of 1/128 have